3-2015

Refraction of Scroll-Wave Filaments at the Boundary between Two Reaction-Diffusion Media

Christian W. Zemlin
Old Dominion University, czemlin@odu.edu

Frency Varghese
Old Dominion University

Marcel Wellner

Arkady M. Pertsov

Follow this and additional works at: https://digitalcommons.odu.edu/bioelectrics_pubs

Part of the Biomedical Engineering and Bioengineering Commons

Refraction of Scroll-Wave Filaments at the Boundary Between
Two Reaction-Diffusion Media

Christian W. Zemlin and Frency Varghese

Department of Electrical and Computer Engineering, Old Dominion University, Norfolk, Virginia 23528, USA
and Frank Reidy Research Center for Bioelectrics, Norfolk, Virginia 23508, USA

Marcel Wellner

Physics Department, Syracuse University, Syracuse, New York 13244, USA

Arkady M. Pertsov

Department of Pharmacology, SUNY Upstate Medical University, Syracuse, New York 13210, USA

We explore the shape and the dynamics of scroll-wave filaments in excitable media with an abruptly changing diffusion tensor, important for cardiac applications. We show that, similar to a beam of light, the filament refracts at the boundary separating domains with different diffusion. We derive the laws of filament refraction and test their validity in computational experiments. We discovered that at small angles to the interface, the filament can become unstable and develop oscillations. The nature of the observed instabilities, as well as overall theoretical and experimental significance of the findings, is discussed.

Three-dimensional excitable media can maintain organized activity in the form of rotating, scroll-shaped waves. Scroll waves have been observed in a wide range of excitable media [1–5], most notably in the heart, where they cause life-threatening arrhythmias [6–8]. They are organized around vortexlike cores, called filaments, that can change shape or break up into multiple interacting fragments [9–11]. Filaments can also become anchored (pinned), giving rise to stationary rotating scroll waves [12–14], which in the heart are linked to sustained arrhythmias.

Excitable media are governed by reaction-diffusion equations. The diffusion coefficient is one of the key parameters, defining the propagation velocity of the excitation wave [15]. In models of the heart, diffusion is described by a tensor, which represents the anisotropic electrical conductance of muscle fibers constituting the myocardial wall [16].

Here, we focus on the shape and the dynamics of anchored filaments in media with a discontinuous change in diffusion. In the heart, such discontinuities correspond to abrupt changes in fiber direction, which are characteristic of the outflow tract [17] and other regions of the myocardium [18]. These regions are linked to arrhythmias [19], but their mechanism remains largely unknown, which makes the investigation of the filament properties in media with discontinuities in diffusion particularly important.

We show that a discontinuity in diffusion makes the filament abruptly change its angle to the interface, reminiscent of the refraction of a light beam at the boundary separating domains with different optical density. There is also a critical angle of the filament to the interface, which cannot be exceeded. Using a generalized geodesic principle [13], we derive analytically the laws of refraction and test their validity computationally for different filament orientations.

Unlike the refraction of an optical beam, filament refraction appears to be a significantly more complex phenomenon manifesting unparalleled dynamic behaviors. Specifically, at small angles of the filament to the interface, we discovered a diffusion-mediated filament instability and oscillatory regimes, in which one segment of the filament abruptly increases in length, overcoming positive filament tension [20], then gradually shortens to erupt again after several scroll-wave rotations. The instability is caused by the gradient force field which is present in the vicinity of the interface and manifests when the filament runs at a small angle to the interface.

The computational experiments are carried out numerically using reaction-diffusion equations with Barkley kinetics [21]:

$$\partial_t u = \epsilon^{-1} u (1 - u)[u - (v + b)/a] + \partial_j (D_{ij} \partial_i u), \quad (1)$$

$$\partial_t v = u - v, \quad (2)$$

where u and v are the activator and inhibitor variable, respectively, and the parameters ϵ, b, and a determine the excitability of the medium.

The diffusion tensor D_{ij} is given different values in the lower ($z < 0$) and upper ($z \geq 0$) parts of the medium, with a discontinuity at the interface. Specifically, we consider two cases, listed in Table I: isotropic diffusion (case I) and anisotropic diffusion with a $\pi/2$ rotation of D in the xy

TABLE I.   Diffusion tensors for cases I and II.

Case	D_{ij} ($z < 0$)	D_{ij} ($z \geq 0$)
I	$d_1 \delta_{ij}$	$d_2 \delta_{ij}$
II	$\mathrm{diag}(d_1, d_2, d_2)$	$\mathrm{diag}(d_2, d_1, d_2)$

plane (case II). In the context of cardiac tissue, case II corresponds to a 90° fiber rotation at $z = 0$.

The scroll wave is initiated between two hemispherical anchors A and B, located at the lower and upper boundaries of the medium. After equilibration, we slowly (quasistatically) increase the ratio of the diffusion coefficients (d_1/d_2, see Table 1), progressively increasing the jump in the diffusion tensor at the interface ($z = 0$), until it reaches the desired value. The resulting filament has two linear segments [see Fig. 1(a)], whose orientation depends on d_1 and d_2. To investigate the entire range of filament orientations with respect to the interface, we also vary the angle between the filament and the interface by gradually moving one of the anchors.
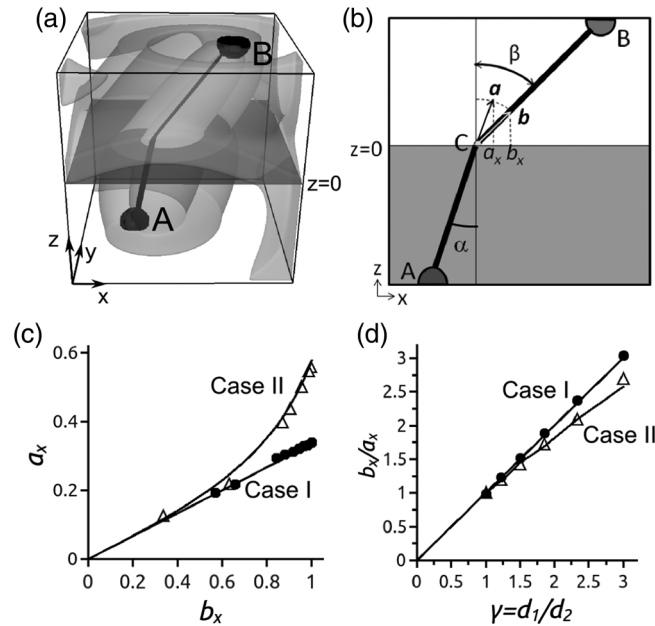

FIG. 1.   Refraction of a scroll-wave filament in a medium with discontinuous diffusion tensor. (a) Snapshot of a scroll wave and its filament in the model given by Eqs. (1) and (2) (case I: $d_1 = 1.5$, $d_2 = 0.5$). The isosurfaces for $u = 0.5$ are shown in transparent gray, the filament and the anchors in black, and the interface between the upper and lower halves in transparent dark gray. The filament is noticeably thinner in the upper region because $d_2 < d_1$. (b) Schematic cross section through the anchor plane ($y = 0$) in (a), explaining our notations. (c) Dependency of a_x on b_x as derived from the geodesic principle (lines) and observed in numerical experiments (symbols) for $\gamma = 3$. (d) Numerical verification of Eqs. (6) and (7) for fixed anchor positions and varying γ.

To compute the filament location we identify the filament tube characterized by reduced amplitude of variable u and determine the center of the tube as described in [12]. We choose medium parameters $\epsilon = 0.02$, $a = 0.9$, $b = 0.05$, which support stable scroll waves with positive filament tension [20]. Medium-size nodes are $100 \times 100 \times 100$ with $\Delta x = 0.25$, for which plane-wave speed is accurate within 3%, and no-flux boundary conditions are imposed.

We first apply the geodesic principle [13] to derive the shape of the stationary filament in cases I and II. According to the geodesic principle, the stationary filament should follow the geodesic with the metric defined as

$$g_{ij} = (\det D)(D^{-1})_{ij}. \tag{3}$$

The symmetry of D requires that the stationary filament consists of two linear segments $\overline{AC}$ and $\overline{CB}$ at different angles α and β to the interface [see Fig. 1(b)]. Let us denote the unit vectors along the segments $\overline{AC}$ and $\overline{CB}$ as $\boldsymbol{a} = (a_x, a_y, a_z)$ for $z < 0$ and $\boldsymbol{b} = (b_x, b_y, b_z)$ for $z \geq 0$, respectively.

Case I.—To find the relationship between α and β, we assume, without loss of generality, that both anchors are located in the plane $y = 0$. Then, the isotropy of D requires that the whole filament stays in this plane ($a_y = b_y = 0$). From Eq. (3), we find the metric tensor g_{ij} for this case:

$$g_{ij} = \begin{cases} (d_1)^2 \delta_{ij} & \text{for } z < 0 \\ (d_2)^2 \delta_{ij} & \text{for } z \geq 0. \end{cases} \tag{4}$$

The geodesic condition then can be written as

$$\delta S = \delta \int \sqrt{g_{ij}dx_i dx_j} = \delta \int_A^C d_1 dl + \delta \int_C^B d_2 dl = 0, \tag{5}$$

from which we obtain the relationship between angles of the upper and lower segments of the filament with the normal [see Fig. 1(b)]:

$$\frac{b_x}{a_x} = \frac{\sin(\beta)}{\sin(\alpha)} = \frac{d_1}{d_2}. \tag{6}$$

Equation (6) is reminiscent of Snell's law for light refraction, with the diffusivities playing the role of refraction indices (this filament refraction is markedly different from the refraction of excitation fronts, which follows the tangent rule [22]).

Case II.—For simplicity, we again assume that $a_y = b_y = 0$. By applying the geodesic principle, we find that a_x can be expressed as the following function of b_x:

$$a_x = \frac{b_x}{\gamma}(1 - b_x^2(1 - 1/\gamma))^{-(1/2)}, \qquad (7)$$

where $\gamma = d_1/d_2$. A full technical derivation of this and a more general case of arbitrary fiber rotation will be presented in a separate publication. Note that, asymptotically at small b_x, Eq. (7) coincides with Eq. (6).

As in the case of light refraction, Eqs. (6) and (7) imply the existence of critical angles α_c for which $\beta = \pi/2$ ($b_x = 1$). In the context of this study, this means that, independently of the anchor's position, the filament will always adapt its shape in such a way that $\alpha \leq \alpha_c$. For case I, $\alpha_c = \arcsin(\gamma^{-1})$, while for case II, $\alpha_c = \arcsin(\gamma^{-1/2})$. The solid lines in Figs. 1(c) and 1(d) show the dependence of a_x on b_x and of the ratio a_x/b_x on γ predicted from Eqs. (6) and (7).

To test the validity of Eqs. (6) and (7), we carry out numerical experiments using the full model [Eqs. (1) and (2)]. The values of a_x and b_x are calculated from the filament coordinates using linear regression applied to the lower and the upper parts of the medium, respectively. The simulation results are superimposed onto the theoretical plots [see Figs. 1(c) and 1(d)]. In both series of computational experiments, we observe excellent agreement with theory.

While holding rather well in a broad range of parameters, the theoretical predictions start failing when $\alpha \to \alpha_c$ and $\beta \to \pi/2$. The deviations are most pronounced in case I. Figure 2 shows the evolution of the filament as the distance of the anchor B from the interface (z_B) gradually decreases. At larger z_B [see panel (a)], the filament consists of two rectilinear fragments, in excellent agreement with the theory. When z_B is reduced from $0.77\lambda_z$ to $0.26\lambda_z$, however,
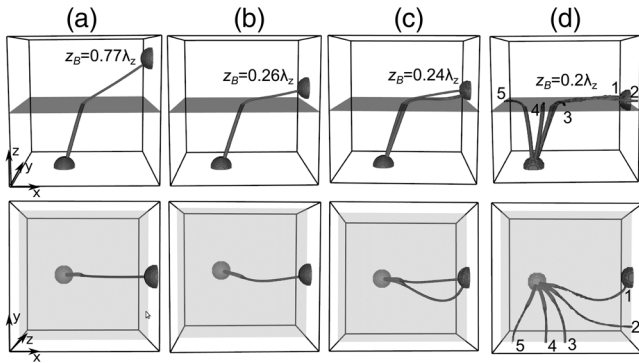
the upper segment of the filament deviates from the geodesic and becomes noticeably curved [see Fig. 2(b)].

As the anchor continues to approach $z = 0$, the deformation increases, and the respective fragment of the filament starts oscillating [Fig. 2(c)]. The oscillation cycle consists of two distinct phases: (1) rapid bulging and moving away from the interface, and (2) slow straightening and approaching the interface. The two filament positions shown in panel (c) represent these two phases. The period of filament oscillations is more than an order of magnitude longer than that of the rotation of the scroll wave. Further reduction in z_B increases the amplitude of oscillation and causes the detachment of the filament from the upper anchor. Attached only at the bottom end, the filament starts clockwise precession around the anchor [see Fig. 2(d)] until it stops in a new position (labeled "5") and resumes oscillations.

It is interesting that during these transformations, the filament shape remains close to the geodesic solution. Indeed, the lower segment of the filament remains rectilinear with $\alpha \approx \alpha_c$. The ratio $\sin(\beta)/\sin(\alpha)$ remains close to γ, as prescribed by Eq. (6) (we use linear regression to approximate the curved filament and compute β). The deviations from the geodesics are less pronounced in case II than in case I (see Fig. 3). Within the range of parameters studied, we do not observe any oscillations and the filament remains attached to both anchors all the way to $z = 0$.

The milder deviations from the theory in case II are due to the fact that, in this case, only two components of the diffusion tensor change at the interface, as opposed to all three in case I. It would be reasonable to expect that in a generalized case II with fiber rotation at the interface of less than $\pi/2$, the deviation from the theory will be even smaller.

In case II, we observe a phenomenon reminiscent of internal reflection [Fig. 3(c)]. When we move the second
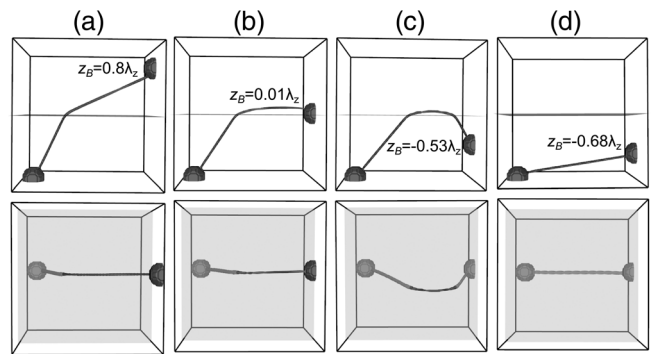

FIG. 2. Filament snapshots (lateral and top views) at different anchor positions in case I, with $d_1 = 1.5$, $d_2 = 0.5$ ($\gamma = 3$). The values of z_B indicate the distance of the anchor B from the interface in units of λ_z, the wavelength of the scroll wave in the z direction. (a) Filament refraction consistent with the geodesic principle. (b) The upper segment of the filament becomes curved. (c) Filament begins to oscillate in the vicinity of the geodesic solution. (d) The filament detaches from anchor B and rotates in the clockwise direction. Numbers show consecutive filament configurations starting from the moment of detachment.

FIG. 3. Refraction and "reflection" of the filament in case II ($\gamma = 3$). Notations as in Fig. 2. (a) The filament consists of two rectilinear fragments consistent with geodesic predictions. (b) At α close α_c, the upper segment of the filament runs almost parallel to the interface. (c) As the anchor B moves below the interface, the filament folds and produces an additional linear segment at an angle close to α_c, reminiscent of internal reflection. (d) Straightening of the filament following further reduction of z_B.
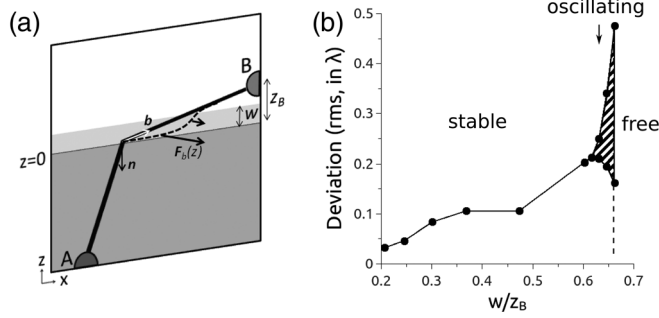
(a)

(b)

FIG. 4.   (a) Schematic illustrating the mechanism of filament deformation at small z_B. The portion of the filament inside the boundary layer of width w experiences a force $\boldsymbol{F}_b$, which pulls it off the xz plane, creating a bulge as indicated by the dashed line. (b) Deviation of the upper filament segment from the straight line as a function of w/z_B (case I, $\gamma = 3$). Deviation was quantified by determining the distance between the predicted and actual filament coordinates in each cross section (yz plane) of the medium and then calculating the root-mean-square deviation. The width of the hatched area indicates the amplitude of oscillations. The dashed vertical line indicates the detachment of the filament from anchor B.

anchor across the interface to the lower half of the medium, we obtain a filament with three segments: the first segment at an angle α close to α_c, the second approximately parallel to the interface, and the third again at an angle close to α_c (a distant analogy to optical total reflection). When the length of the central fragment becomes very small, the filament detaches from the interface and acquires a rectilinear shape [Fig. 3(d)].

The deviations of the filament shape from the geodesic and the complex filament dynamics at small angles to the interface are the result of a short-range force $\boldsymbol{F}_b$ which affects the filament in the vicinity of the boundary separating regions with different diffusion [see Fig. 4(a)]. Such a force is present at any boundary separating domains with different parameters [23]. In our case, $\boldsymbol{F}_b(z) \propto |\boldsymbol{n} \times \boldsymbol{b}|$, where $\boldsymbol{n}$ is the normal to the interface pointing in the direction of greater diffusivity. By analogy with two-dimensional cases [23,24], it is reasonable to expect that the spatial range of $\boldsymbol{F}_b$ is of the order of the filament radius, $w = \lambda_z/2\pi$. Parts of the filament located outside the boundary layer defined by w remain unaffected by $\boldsymbol{F}_b$ [see Fig. 4(a)].

The portion of the filament experiencing $\boldsymbol{F}_b$ is therefore w/z_B. For small β the affected portion is small and has little effect on the filament angle. As β increases, so does w/z_B, until the entire segment $\overline{CB}$ is affected ($w/z_B = 1$) as β approaches $\pi/2$. $\boldsymbol{F}_b$ makes the filament drift, while the anchor prevents the end of the filament from moving. This causes the filament deviation from the rectilinear shape and the development of curvature-related normal and binormal forces which contribute to subsequent filament dynamics [12].

Figure 4(b) shows the average deviation of the filament from the straight line as a function of w/z_B for case I. Indeed, the deviation is small when $w/z_B \ll 1$ and dramatically increases as w/z_B approaches 1. Oscillations start as $w/z_B \approx 0.63$, whereas complete detachment occurs at $w/z_B \approx 0.67$. The gradual rise of oscillation amplitude suggests that the bifurcation is supercritical, while the narrow range of w/z_B in which we see deviations is likely the result of the strong dependence of F_b on z.

Our findings have important implications with regard to utility of the geodesic principle [25,26]. The geodesic principle enables the prediction of the shape of the stationary filament exclusively from the diffusion tensor, without considering the kinetic parameters of the medium. The validity of the geodesic principle was proven only for small filament curvatures [27] which limited its practical application. Our study shows that for practical purposes, with the exceptions mentioned above, the requirement of small filament curvature can be relaxed. Computer simulations clearly show that despite significant curvature of the filament near the interface, its shape remains consistent with the geodesic predictions. Considering that this study focuses on the most extreme case of discontinuous diffusion, it is reasonable to expect that the agreement will be even better in the majority of cases where the diffusion changes more gradually.

In summary, we demonstrated that an anchored filament refracts at the boundary separating domains with an abruptly changing diffusivity tensor. In the particular case of domains with isotropic diffusion, the refraction law is reminiscent of Snell's law in geometrical optics. We showed that the condition of small filament curvature used for the derivation of the minimal principle for practical purposes can be relaxed, which significantly extends the utility of the geodesic approximation. Finally, we discovered oscillatory regimes, and instabilities resulting from abrupt changes in anisotropy that shed new light onto the role of the abrupt changes of anisotropy in the development and dynamics of cardiac arrhythmias.

[1] A. T. Winfree, Science **181**, 937 (1973).
[2] F. Siegert and C. J. Weijer, Proc. Natl. Acad. Sci. U.S.A. **89**, 6433 (1992).
[3] B. J. Welsh, J. Gomatam, and A. E. Burgess, Nature (London) **304**, 611 (1983).
[4] T. Bánsági and O. Steinbock, Chaos **18**, 026102 (2008).
[5] S. Alonso, F. Sagués, and A. S. Mikhailov, Science **299**, 1722 (2003).
[6] I. R. Efimov, V. Sidorov, Y. Cheng, and B. Wollenzier, J. Cardiovasc. Electrophysiol. **10**, 1452 (1999).
[7] B. G. Mitrea, M. Wellner, and A. M. Pertsov, in *Engineering in Medicine and Biology Society, 2009. EMBC 2009. Annual International Conference of the IEEE* (IEEE, 2009), pp. 4194–4197.

[8] W. T. Baxter, S. F. Mironov, A. V. Zaitsev, J. Jalife, and A. M. Pertsov, Biophys. J. **80**, 516 (2001).

[9] A. V. Panfilov, Chaos **8**, 57 (1998).

[10] R. M. Zaritski, S. F. Mironov, and A. M. Pertsov, Phys. Rev. Lett. **92**, 168302 (2004).

[11] F. Fenton and A. Karma, Phys. Rev. Lett. **81**, 481 (1998).

[12] M. Vinson, A. M. Pertsov, and J. Jalife, Physica D (Amsterdam) **72**, 119 (1994).

[13] M. Wellner, C. Zemlin, and A. M. Pertsov, Phys. Rev. E **82**, 036122 (2010).

[14] Z. A. Jiménez, B. Marts, and O. Steinbock, Phys. Rev. Lett. **102**, 244101 (2009).

[15] J. Keener, SIAM J. Appl. Math. **39**, 528 (1980).

[16] C. S. Henriquez, Critical Reviews in Biomedical Engineering **21**, 1 (1993).

[17] M. Burgess, B. Steinhaus, K. Spitzer, and P. Ershler, Circ. Res. **62**, 233 (1988).

[18] G. X. Yan, W. Shimizu, and C. Antzelevitch, Circulation **98**, 1921 (1998).

[19] R. J. Kim, S. Iwai, S. M. Markowitz, B. K. Shah, K. M. Stein, and B. B. Lerman, J. Am. Coll. Cardiol. **49**, 2035 (2007).

[20] V. N. Biktashev, A. V. Holden, and H. Zhang, Phil. Trans. R. Soc. A **347**, 611 (1994).

[21] D. Barkley, Physica D (Amsterdam) **49**, 61 (1991).

[22] O. Mornev, JETP Lett. **80**, 721 (2004).

[23] I. V. Biktasheva, D. Barkley, V. N. Biktashev, and A. J. Foulkes, Phys. Rev. E **81**, 066202 (2010).

[24] C. W. Zemlin and A. M. Pertsov, Phys. Rev. Lett. **109**, 038303 (2012).

[25] M. Wellner, O. Berenfeld, J. Jalife, and A. M. Pertsov, Proc. Natl. Acad. Sci. U.S.A. **99**, 8015 (2002).

[26] K. H. W. J. tenTusscher and A. V. Panfilov, Phys. Rev. Lett. **93**, 108106 (2004).

[27] H. Verschelde, H. Dierckx, and O. Bernus, Phys. Rev. Lett. **99**, 168104 (2007).